# UC Davis

## UC Davis Previously Published Works


### Title

Validation of a Contour Method Single-Measurement Uncertainty Estimator


### Permalink

https://escholarship.org/uc/item/0x60c4pz



### Journal

Experimental Mechanics, 58(5)

### ISSN

0014-4851



### Authors

Olson, MD
DeWald, AT
Hill, MR



### Publication Date

2018-06-01

### DOI

10.1007/s11340-018-0385-4

Peer reviewed



eScholarship.org Powered by the California Digital Library
University of California

# Validation of a Contour Method Single-Measurement Uncertainty Estimator

Mitchell D. Olson*, Adrian T. DeWald, and Michael R. Hill

*Hill Engineering, LLC, 3083 Gold Canal Drive, Rancho Cordova, CA, USA*

Submitted to *Experimental Mechanics*, October 2017; Accepted February 2018
Appeared as Olson, M.D., DeWald, A.T. & Hill, M.R. Exp Mech (2018) 58: 767.
https://doi.org/10.1007/s11340-018-0385-4

## ABSTRACT

This work validates an analytical single-measurement uncertainty estimator for contour method measurement by comparing it with a first-order uncertainty estimate provided by a repeatability study. The validation was performed on five different specimen types. The specimen types cover a range of geometries, materials, and stress conditions that represent typical structural applications. The specimen types include: an aluminum T-section, a stainless steel plate with a dissimilar metal slot-filled weld, a stainless steel forging, a titanium plate with an electron beam slot-filled weld, and a nickel disk forging. For each specimen, the residual stress was measured using the contour method on replicate specimens to assess measurement precision. The uncertainty associated with each contour method measurement was also calculated using a recently published single-measurement uncertainty estimator. Comparisons were then made between the estimated uncertainty and the demonstrated measurement precision. These results show that the single-measurement analytical uncertainty estimate has good correlation with the demonstrated repeatability. The spatial distributions of estimated uncertainty were found to be similar among the conditions evaluated, with the uncertainty relatively constant in the interior and larger along the boundaries of the measurement plane.

*Keywords: Residual stress measurement, contour method, uncertainty, precision, repeatability*

## 1. INTRODUCTION

Experimental data and their associated uncertainty are fundamental for experimental testing, as well as for validation of engineering models. Experimental validation is the process of determining the degree to which a model is an accurate representation of the real-world from the perspective of the intended uses of the model [1] and experimental uncertainty effectively establishes the resolution at which such comparisons can be made [2]. Similarly, when experimental data are used to predict an output, the experimental data uncertainty will determine the bounds of the predicted output. The bounds

* Corresponding author. *E-mail address:* molson@hill-engineering.com

of the predicted output will ultimately determine whether the experimental data are useful for predicting a real-world phenomenon. Therefore, uncertainty is important for all measurements since it determines whether a given measurement is useful for its intended purpose.

The contour method is a residual stress measurement technique that provides a two-dimensional map of residual stress on a given measurement plane. The two-dimensional residual stress map provided by the contour method has been found to be useful for validating computation weld analyses [3,4,5], predicting fatigue performance [6], evaluating the effectiveness of manufacturing processes like peening [7,8], cold hole expansion [9], and welding [10]. Although, the contour method has proven useful, most prior work lacks an uncertainty estimate for the contour method data.

Recently, a single-measurement uncertainty estimator was developed for the contour method [11]. The objective of the present work is to validate this uncertainty estimator by assessing the level of correlation between the uncertainty estimate and a first-order uncertainty estimate. The first order uncertainty estimate is determined with a set of repeatability studies that quantify the measurement precision of the contour method over a range of conditions. Measurements were performed on specimen types that include a range of geometries, materials, and residual stress conditions. For each specimen type, the residual stress was measured on replicate specimens using the contour method to establish measurement precision. The single-measurement uncertainty estimate associated with each contour method measurement was also calculated. Comparisons were then made between the estimated uncertainty and the demonstrated precision to validate the uncertainty estimator.

## 2. METHODS

This work includes multiple steps. First, five test specimens were designed and manufactured. The specimen types cover a range of geometry, material, and residual stress condition that represent a range of structural applications. Replicate specimens of each type were produced (between 5 and 10 replicate

specimens for each specimen type). Second, residual stress measurements were performed on each specimen type using the contour method. Third, the uncertainty associated with each single measurement was estimated. Fourth, the precision of the contour method was calculated for each specimen type. Finally, comparisons were made between the estimated uncertainty and the demonstrated precision for each specimen type. Details of the specimens, contour method, uncertainty estimation, and data comparisons follow. A more complete description of the repeatability studies can be found elsewhere [12].

### *2.1. Test specimen manufacture*

Five different test specimen types were manufactured: an aluminum T-section (10 specimens), a stainless steel plate with a dissimilar metal (DM) slot-filled weld (5 specimens), a titanium plate with an electron beam (EB) slot-filled weld (6 specimens), a stainless steel forging (6 specimens), and a nickel disk forging (6 specimens).

The aluminum T-section specimen type was fabricated from 7050-T7451 aluminum plate (cut into bars) that had been stress relieved by stretching during forming. The original bars had a length of 762 mm (30.0 in), a height of 82.55 mm (3.25 in), and a width of 82.55 mm (3.25 in). The bars were heat treated, including a quench, to induce high residual stress indicative of the -T74 temper. The heat treatment used the recipe described in [13] and consists of heating the samples to 477°C (890°F) for 3 hours, quenching in room temperature water, artificial aging at 121°C (250°F) for 8 hours followed by additional aging at 177°C (350°F) for 8 hours. T-sections were then machined from the bars to represent an airframe structural member. Each T-section had a length of 254 mm (10.0 in), a height of 50.8 mm (2.0 in), a width of 82.55 mm (3.25 in), and a flange thicknesses of 6.35 mm (0.25 in) as shown in Figure 1.

The stainless steel dissimilar metal (DM) weld specimen type was fabricated from one long plate made of high-strength 316L stainless steel. The plate had a 25.4 mm (1.0 in) by 152.4 mm (6.0 in) cross-section and a length of 1.22 m (48.0 in). A slot was machined along the entire length of the plate with a 9.53 mm (0.375 in) groove depth, a 19.05 mm (0.75 in) width, and a 70º root angle. The groove and plate cross-section can be seen in Figure 2. Before filling in the slot with weld material, a continuous 7.94 mm (0.313 in) fillet weld was applied along the 1.22 m edges to join the plate to a stiff fixture, to add restraint during the welding process. The slot was filled with 8 passes, each applied along the entire length of the plate using an automated process and 0.89 mm (0.035 in) diameter A52M (ERNiCrFe-7A) wire. Following welding, the fillet welds were machined away to release the plate from the backing fixture and the ends of the plate were removed to eliminate the inconsistent weld bead geometry at the start and stop of the weld.

The titanium alloy electron beam (EB) welded plate specimen type was fabricated using one long plate made of Ti-6Al-4V, with similar geometry to the stainless steel DM welded plate (same cross-section and slot dimensions). The groove was filled along the entire length of the plate with 8-passes of 3.18 mm (0.125 in) diameter Ti-6Al-4V wire. After completion of the weld, the plate was sectioned into 101.6 mm (4.0 in) long pieces, as shown in Figure 3. These samples were representative of a typical wire fed additive manufacturing process in the as-manufactured condition (prior to thermal stress relief).

The 304L stainless steel forging specimen type is roughly hemi-spherical with an outer diameter of 73.7 mm (2.9 in). They include a forged internal cavity with an inner diameter of 30.5 mm (1.2 in), and a height of 50.8 mm (2.0 in) (Figure 4). The samples were produced using a multi-stage forging process. The sample billets were heated to 980°C (1800°F) for 60 min, die pressed to 75% of their original height in a hydraulic press, cooled to room temperature, heated to 1750°F for 60 min, and subjected to a high energy rate forging operation. The samples were then cooled to room temperature, annealed at 955°C

(1750°F) for 30 min, and water quenched. The final processing steps consisted of reheating the samples to 845°C (1550°F) for 60 min, a final high energy rate forging operation, followed by a final water quench.

The sample type comprised of a nickel based super-alloy (Udimet-720Li) forging had a diameter of 151.20 mm (5.95 in) and a maximum height of 70.41 mm (2.77 in), as shown in Figure 5. The samples were forged and heat treated, including a quench, to achieve desired mechanical properties. The heat treatment consisted of pre-heating the samples to 1080°C (1975°F), forging to a nominally finished shape, solution heat treating at 1105°C (2020°F), and oil quenching. The samples were then stabilized at 760°C (1400°F) for 8 hours, air cooled, aged at 650°C (1200°F) for 24 hours and then air cooled to room temperature. The forgings were sectioned in half prior to the contour method measurements (to allow for more replicate measurements as discussed in [12]). The stress release from sectioning the forging sample in half was included in the reported stress values by using a supplemental stress analysis as described in [14]. The stress analysis used measured strain gage data from eight hoop sensing, strain gages placed along the ID and OD of the disk at the subsequent measurement plane (180° from the sectioning plane).

### *2.2. Contour method measurements*

The contour method is a stress-relaxation residual stress measurement technique whose theoretical foundation was established by Prime [15]. A contour method measurement will cut a part along a given measurement plane and surface deformations will occur as a result of residual stress redistribution. The surface profiles at the cut plane can be measured and are analogous to the residual stress before cutting. When the negative of the measured surface profiles are applied as boundary conditions to an elastic finite element model of the part, the residual stress released normal to the cutting plane can be

determined. Prime and DeWald [16] have established good practices for experimental steps required for the contour method.

Each contour method measurement followed nominally the same procedure. Each specimen was cut in two using wire electric discharge machining (EDM) while rigidly clamped to the EDM tool frame. Following cutting, a laser scanning profilometer was used to measure the surface height profiles normal to the cut plane as a function of in-plane position for each of the two opposing cut surfaces. Surface height data were taken on a grid of points with spacing ranging from 100 to 200 μm in each direction. The two surface profiles were aligned, averaged on a common grid, and fit to a smooth bivariate analytical function. The residual stress release on each measurement plane was determined by applying the negative of the smoothed surface profile as a set of displacement boundary conditions to the cut face of a linear elastic finite element model of the cut part. The models used the elastic material properties given in Table 1.

### *2.3. Contour method uncertainty estimation*

The uncertainty for each contour method measurement was estimated following the approach outlined in [11]. The uncertainty estimate accounts for two main, random uncertainty sources present in contour method measurements, including the uncertainty associated with random noise in the surface height profiles called the *displacement error* and the uncertainty associated with choosing a specific analytical model to fit the surface profiles called the *model error*.

The displacement error is estimated using a Monte Carlo approach that applied normally distributed noise to the each of the original measured surface height profiles. The normally distributed noise was previously found to approximate the surface roughness that arises from EDM cutting [11]. Stress results were found with five different sets of random noise added to the surface height profiles and the standard

deviation of those five residual stress results, at each spatial location, was taken as the displacement error.

The model error is estimated by taking the standard deviation of the residual stress results using displacement surface profiles that have been fit with different analytical models (centered around what was determined to be the best fit). Each case used a different number of fitting coefficients. The total uncertainty was then taken as the root-sum-square of the displacement and model errors with a minimum value of uncertainty set as a floor. The floor used in all cases was the mean of the total uncertainty, which was evaluated over a grid with roughly equal spacing. The uncertainty estimate is assumed to have a normal distribution, which implies that one standard deviation represents a 68% confidence interval.

### *2.4. Comparison of uncertainty and precision*

The purpose of the single measurement uncertainty estimate is to be able to accurately estimate the random uncertainty that is present during a contour method measurement. To assess whether the uncertainty estimate was accurately estimating random uncertainty, each pointwise measurement result ± its associated uncertainty was compared with the mean of the repeatability study at the same location. The mean was chosen as the reference value because it is expected to be the most representative of the underlying residual stress field (and the difference between the mean and each measured result is a reasonable representation of the random measurement error, assuming each specimen has a similar initial residual stress state). Every measurement point on the cross-section was assigned to one of two groups depending on whether (positive bin) or not (negative bin) the range of residual stress values at that location defined by the measured stress ± its associated uncertainty included the population mean. Since both uncertainty sources were assumed to have normal distributions, and

since the uncertainty estimate is based on one standard deviation, 68% of the points on the cross section are expected to fall within the positive bin.

## 3. RESULTS

Results for each of the five specimen conditions are summarized in Figure 6 through Figure 26. For each specimen condition the following results are shown: 1) a fringe plot of a typical single measurement result, 2) the estimated uncertainty associated with that measurement result along with the individual contributions to the uncertainty, 3) the mean of each specimen population, 4) a line plot of residual stress versus position showing each individual measurement, the population mean, and the associated uncertainty for one of the measurements, and 5) a fringe plot showing the locations on the cross-section where the comparison of uncertainty and precision shows a positive or negative result. A summary of tabulated uncertainty and repeatability standard deviation statistical values for each specimen type is given in Table 2.

The longitudinal stress in the aluminum T-section has compressive stress at the left and right edges of the bottom flange (min ≈ -240 MPa) and at the top of the center flange (≈ -70 MPa) with tensile stress at the intersection of the bottom and center flanges (max ≈ 100 MPa) (Figure 6a). The mean of the population is shown in Figure 6b. The uncertainty in the aluminum T-section is shown in Figure 7. The model error (Figure 7a) is largest along the part boundary ($95^{th}$ percentile is at 21.8 MPa), and at the intersection of the bottom and central flange. The displacement error (Figure 7b) is also largest along the part boundary ($95^{th}$ percentile is at 3.4 MPa), at the left, right, and top edges. The displacement error is much smaller than the model error. The total uncertainty essentially has the same distribution as the model error ($95^{th}$ percentile is at 22.0 MPa) with a 9.9 MPa floor covering a large portion of the cross-section (Figure 7c).

The comparison between uncertainty and precision was positive at 95.1% of points as shown in Figure 8 (similar comparisons for the other specimens showed a range of 99.2% to 85.3% and the mean of all specimens is 94.9%). Furthermore, the measured residual stress for all repeat measurements along the $x$-direction at $y$ = 3.18 mm and along the $y$-direction at $x$ = 40.52 mm is shown in Figure 9. The line plots show that the uncertainty estimate is reasonable at predicting the spread in the measurement data (that is related to random measurement error).

### *3.1. Stainless steel DM welded plate*

The longitudinal stress in the stainless steel DM welded plate has tensile stress in the weld area and heat-affected zone (max ≈ 380 MPa) and near $y$ = 0 at the left and right edges of the plate where the plate was tack welded (max ≈ 400 MPa). There is compensating compressive stress toward the top of the plate at the left and right edges (min ≈ -260 MPa) (Figure 10a and Figure 10b). The uncertainty in the stainless steel DM welded plate is shown in Figure 11. The model error (Figure 11a) is largest along the part boundary ($95^{th}$ percentile is at 41.0 MPa). The displacement error (Figure 11b) is also largest along the part boundary and at the left, right, and top edges ($95^{th}$ percentile is at 11.8 MPa). The displacement error is much smaller than the model error. The total uncertainty has nearly the same distribution as the model error ($95^{th}$ percentile is at 42.5 MPa) with a 17.5 MPa floor covering most of the cross-section (Figure 11c).

The comparison between the uncertainty and precision was positive at 80.3% of points as shown in Figure 12 (comparisons for the other specimens showed a range of 83.3% to 65.1% and the mean of all specimens is 74.1%). Furthermore, the measured residual stress for all repeat measurements along the $x$-direction at $y$ = 19.05 mm and along the $y$-direction at $x$ = 76.2 mm is shown in Figure 13. The line plots show that the uncertainty estimate is reasonable at predicting the spread in the measurement data.

### *3.2. Titanium electron beam welded plate*

The longitudinal stress in the titanium EB welded plate has tensile stress in the weld area (max ≈ 350 MPa) and compensating compressive stress in the heat-affected zone (min ≈ -200 MPa) (Figure 14a and Figure 14b). The uncertainty in the titanium EB welded plate is shown in Figure 15. The model error (Figure 15a) is largest along the part boundary ($95^{th}$ percentile is at 27.6 MPa). The displacement error (Figure 15b) is also largest along the part boundary ($95^{th}$ percentile is at 10.8 MPa). As was the case for the other samples, the displacement error is much smaller than the model error and the total uncertainty mirrors the model error distribution ($95^{th}$ percentile is at 32.5 MPa) with a 12.2 MPa floor covering most of the cross-section (Figure 15c).

The comparison between the uncertainty and precision is positive at 94.5% of points as shown in Figure 16 (comparison values ranged from 98.0% to 92.1% for the other specimens with a mean of 95.9%). The measured residual stress for all repeat measurements along $x$-direction at $y$ = 20.32 mm and along the $y$-direction at $x$ = 68.15 mm is shown in Figure 17. The line plots show that the uncertainty estimate is reasonable at predicting the spread in the measurement data.

### *3.3. Stainless steel forging*

The hoop stress in the stainless steel forging has tensile stress along the boundary of the forging cavity (max ≈ 340 MPa) and compensating compressive stress around the outer diameter of the forging (min ≈ -260 MPa) (Figure 18a). The measured stress is nominally consistent for five of the six repeat measurements, and the one outlier measurement was omitted from the calculation of the mean (Figure 18b). The outlying measurement had significantly larger stresses near the inner forging cavity (up to 200 MPa larger than the other measurements). The large differences in this measurement were assumed to be primarily related to an inconsistency in the forging process rather than measurement variation, and therefore the outlying result was omitted from the repeatability study. The uncertainty in the stainless

steel forging is shown in Figure 19. The model error (Figure 19a) is largest along the part boundary and is significantly larger than for the other experiments, especially along the boundary of inner forging cavity (95$^{th}$ percentile is at 132.0 MPa). The displacement error (Figure 19b) is also largest along the part boundary (95$^{th}$ percentile is at 6.7 MPa), at the top edges. Consistent with the other cases, the displacement error is much smaller than the model error and the total uncertainty essentially has the same distribution as the model error. The total uncertainty has a 95$^{th}$ percentile at 132.2 MPa) and a large 44.9 MPa floor covering most of the cross-section (Figure 19c).

The comparison between the uncertainty and precision was positive at 99.8% of points as shown in Figure 20 (similar comparisons for the other specimens showed a range of 99.8% to 52.4% and the mean of all specimens is 89.5%). The near totality of points with a positive comparison result is due to the very large uncertainty floor, which is driven by the high uncertainties at the forging cavity interior. The measured residual stress for all repeat measurements (omitting the outlier) along the $x$-direction at $y$ = 19.05 mm and along the $y$-direction at $x$ = 0 is shown in Figure 21. The line plots show that the uncertainty estimate conservatively predicts the spread in the measurement data.

### *3.4. Nickel disk forging*

The hoop stress in the nickel disk forging is tensile towards the center of the forging inner diameter (max ≈ 450 MPa) and has compensating compressive stress toward the forging outer diameter and along the top and bottom of the forging (min ≈ -580 MPa) (Figure 22a and Figure 22b). The stress release when sectioning the part in half significantly contributes to the total hoop stress. The sectioning stress has a bending moment type stress distribution with tensile stress towards the ID (min = 550 MPa) and compressive stress towards the OD (min = 230 MPa). The uncertainty in the nickel forging is shown in Figure 24. The model error (Figure 24a) is largest along the part boundary (95$^{th}$ percentile is at 54.2 MPa). The displacement error (Figure 24b) is also largest along the part boundary (along the inner and

outer diameter as well as the top and bottom edges) ($95^{th}$ percentile is at 11.2 MPa). As was found in the other cases, the displacement error is much smaller than the model error and the total uncertainty is similar to the model error ($95^{th}$ percentile is at 55.5 MPa) with a 20.0 MPa floor covering most of the cross-section (Figure 24c).

The comparison between uncertainty and precision was positive at 76.2% of points as shown in Figure 25 (the comparisons for the other specimens produced positive results at 76.6% to 50.0% and the mean of all specimens is 65.6%). The measured residual stress for all repeat measurements along $x$-direction at $y$ = 35.15 mm and along the $y$-direction at $x$ = 25.4 mm is shown in Figure 26. The line plots show that the uncertainty estimate reasonably predicts the spread in measurement data.

## 4. DISCUSSION

For each case investigated here, the comparison between the uncertainty estimate and the measurement precision produced a positive result at a significantly greater number of points than expected (68%). On average, the comparison was positive at 94.9% of points for the aluminum T-section, 73.3% for the stainless steel DM welded plate, 95.9% for the titanium EB welded plate, 97.0% for the stainless steel forging, and 65.6% for the nickel disk forging. This suggests that the uncertainty estimator is conservative. The estimator is likely to have additional conservatism that stems from real differences among the residual stresses within each population of specimens, since such specimens cannot be made precisely identical, that increases the observed repeatability standard deviation. In summary, the single measurement uncertainty estimator was found to provide a conservative estimate of contour method measurement precision.

Overall, the uncertainty estimate yields similar trends for all cases. Both the model error and the displacement error had spatial distributions with larger uncertainties along the part boundaries and the displacement error was significantly smaller than the model error. The total uncertainty had nearly the

same distribution as the model error, but with most points in the interior having an uncertainty that was determined by the floor.

Histograms of the uncertainty prior to adding the uncertainty floor were created for each case and the histogram for the stainless steel DM welded sample is shown in Figure 27a. The histogram shows that the data roughly follow a log-normal trend and that a portion of the data has large uncertainties. The data were further separated into two groups based on proximity to the perimeter of the cross-section. The near-surface group contained all the points within 1 mm of the part boundary and the interior group contained the remaining points. The data from each bin were fit to a lognormal distribution as shown in Figure 27b (where the dashed lines show a lognormal distribution and the points show the distribution of the data). The results show that the near-surface points contained most of the high magnitude uncertainties and each data range fits a log-normal distribution reasonable well away from low and high probabilities. Furthermore, when the data are separated into near-surface and interior groups, each fits a log-normal distribution better than did the combined population. Other distances to define the near-surface group were tested (0.5 and 2 mm) and it was found that the results for 1 mm capture most of the high uncertainty points better than using a 0.5 or 2 mm distance to define the groups. Similar results were found in other specimens, but are not shown for brevity.

Although the trends in uncertainty were similar between cases, the magnitude of the uncertainty estimate was different between the cases. The total uncertainty estimate for near-surface (within 1 mm) and interior points is plotted for each case in Figure 28a. When the total uncertainty estimate of the near surface and interior points was normalized by the elastic modulus (Figure 28b) both appear to be nominally constant and follow a trend that can be approximated by $250 \times 10^{-6}E$ for near-surface points and $125 \times 10^{-6}E$ for interior points, where $E$ is the elastic modulus. The stainless steel forging appears to

be an outlier, with high uncertainty. We attribute the high uncertainty to areas of high stress magnitude and high stress gradient near the cavity inner wall, which drive up the model error.

The displacement error for all the cases has a minor contribution to the total uncertainty estimate. To quantify the effect of the displacement error on the total uncertainty, the total uncertainty was calculated with and without the displacement error and difference between the floor and 95$^{th}$ percentile was determined for each case. The difference in the floor of the uncertainty estimate with and without the displacement error is 0.1 MPa (1.4 x $10^{-6}E$) for the aluminum T-section, 1.0 MPa (5.0 x $10^{-6}E$) for the stainless steel DM welded plate, 1.3 MPa (11.8 x $10^{-6}E$) for the titanium EB welded plate, 0.1 MPa (7.0 x $10^{-6}E$) for the stainless steel forging, and 0.6 MPa (3.0 x $10^{-6}E$) for the nickel disk forging. The difference in the 95$^{th}$ percentile of the uncertainty estimate with and without the displacement error is 0.2 MPa (2.8 x $10^{-6}E$) for the aluminum T-section, 1.5 MPa (7.5 x $10^{-6}E$) for the stainless steel DM welded plate, 4.9 MPa (44.5 x $10^{-6}E$) for the titanium EB welded plate, 0.3 MPa (1.5 x $10^{-6}E$) for the stainless steel forging, and 1.3 MPa (6.4 x $10^{-6}E$) for the nickel disk forging. Since the effect of the displacement error on both the floor and 95$^{th}$ percentile of the total uncertainty estimate was less than 1% of the stress range, the displacement error can be omitted from the uncertainty estimate calculation without a significant impact on the uncertainty estimate. The model error is the larger contributor to the total uncertainty because the analytical models that are used to calculate the model error can change the fit surface displacement profile relatively rapidly as the number of coefficients changes between analytical models, whereas noise in the displacement profiles has a small bearing on the fit profile for a given analytical model.

The dominance of the model error term is interesting and likely also applies in other residual stress measurement methods. In slitting and hole drilling, often the uncertainty is only estimated using a displacement error like estimator (*strain error/uncertainty* in [17]) and omits the *model*

*error/uncertainty* due to the basis functions used in the stress calculation procedure. This could potentially lead to under reported uncertainties if the model error/uncertainty is significant in those measurement techniques.

## 5. SUMMARY/CONCLUSIONS

This work compared a recently developed single-measurement uncertainty estimator for the contour method with measurement precision for five experimental conditions. The experimental cases covered a range of sample geometry, material, and stress condition: an aluminum T-section, a stainless steel plate with a dissimilar metal slot-filled weld, a stainless steel forging, a titanium plate with an electron beam slot-filled weld, and a nickel disk forging. The comparison checked whether the uncertainty estimator enables favorable comparison with the mean stress found from a set of nominally identical repeated measurements. The results of the comparison showed the uncertainty estimate to provide a reasonable approximation of the random uncertainty present in a single contour method measurement. The model error was the largest contributor to the total uncertainty and the displacement error was found to have a negligible contribution. The floor and 95$^{th}$ percentile of the total uncertainty estimate was found to be 9.9 and 22.0 MPa for the aluminum T-section, 17.5 and 41.0 MPa for the stainless steel DM welded plate, 12.2 and 32.5 MPa for the titanium EB welded plate, 44.9 and 132.2 MPa for the stainless steel forging, and 20.0 and 55.5 MPa for the nickel disk forging, respectively. The total uncertainty was found to be related to the elastic modulus with a value of approximately 250 x $10^{-6}E$ for points within 1 mm of the part boundary and 125 x $10^{-6}E$ for interior points.

## 6. ACKNOWLEDGEMENTS

The authors acknowledge, with gratitude, the U.S. Air Force for providing financial support for this work (contract FA8650-14-C-5026). We would also like to acknowledge Steve McCracken from the Electric Power Research Institute for suppling and fabricating the stainless steel plate with a dissimilar

metal slot-filled weld, Thomas Reynolds from Sandia National Laboratory for providing the stainless steel forgings, and Brian Streich from Honeywell for providing the nickel disk forgings.

## REFERENCES

[1] ASME, "V&V 10-2006: guide for verification and validation in computational solid mechanics," *New York: American Society of Mechanical Engineers (ASME)*, 2006.

[2] H. W. Coleman and W. G. Steele, in *Experimentation, Validation, and Uncertainty Analysis for Engineers*, 3rd ed., Hoboken, New Jersey: John Wiley & Sons, Inc., 2009.

[3] M. C. Smith, A. C. Smith, R. Wimpory, and C. Ohms, "A review of the NeT Task Group 1 residual stress measurement and analysis round robin on a single weld bead-on-plate specimen," *Int. J. Pressure Vessels Piping*, vol. 120–121, pp. 93–140, 2014/8.

[4] H. J. Rathbun, L. F. Fredette, P. M. Scott, A. A. Csontos, and D. L. Rudland, "NRC Welding Residual Stress Validation Program International Round Robin Program and Findings," in *ASME 2011 Pressure Vessels and Piping Conference*, 2011, pp. 1539–1545.

[5] M. N. Tran, M. R. Hill, and M. D. Olson, "Further Comments on Validation Approaches for Weld Residual Stress Simulation," in *ASME 2015 Pressure Vessels and Piping Conference*, 2015, pp. V06BT06A071–V06BT06A071.

[6] O. Hatamleh, "A comprehensive investigation on the effects of laser and shot peening on fatigue crack growth in friction stir welded AA 2195 joints," *Int. J. Fatigue*, vol. 31, no. 5, pp. 974–988, 2009/5.

[7] L. Hacini, N. Van Lê, and P. Bocher, "Evaluation of Residual Stresses Induced by Robotized Hammer Peening by the Contour Method," *Exp. Mech.*, vol. 49, no. 6, p. 775, Dec. 2008.

[8] S. D. Cuellar, M. R. Hill, A. T. DeWald, and J. E. Rankin, "Residual stress and fatigue life in laser shock peened open hole samples," *Int. J. Fatigue*, vol. 44, pp. 8–13, 2012.

[9] Y. Zhang, M. E. Fitzpatrick, and L. Edwards, "Measurement of the residual stresses around a cold expanded hole in an EN8 steel plate using the contour method," in *Materials science forum*, 2002, vol. 404, pp. 527–534.

[10] W. Woo, G. B. An, E. J. Kingston, A. T. DeWald, D. J. Smith, and M. R. Hill, "Through-thickness distributions of residual stresses in two extreme heat-input thick welds: A neutron diffraction, contour method and deep hole drilling study," *Acta Mater.*, vol. 61, no. 10, pp. 3564–3574, Jun. 2013.

[11] M. D. Olson, A. T. DeWald, M. R. Hill, and M. B. Prime, "Estimation of Uncertainty for Contour Method Residual Stress Measurements," Exp. Mech., vol. 55, no. 3, pp. 577–585, 2014.

[12] M.D. Olson, A.T. DeWald, M.R. Hill, "Repeatability of contour method residual stress measurements," Submitted to Experimental Mechanics, 2016.

[13] SAE Aerospace, “Aerospace Material Specification 4342: Aluminum Alloy Extrusions: Solution Heat Treated, Stress Relieved, Straightened, and Overaged,” 2006.

[14] W. Wong and M. R. Hill, “Superposition and Destructive Residual Stress Measurements,” Exp. Mech., vol. 53, no. 3, pp. 339–344, Mar. 2013.

[15] M. B. Prime, “Cross-Sectional Mapping of Residual Stresses by Measuring the Surface Contour After a Cut,” J. Eng. Mater. Technol., vol. 123, no. 2, pp. 162–168, Apr. 2001.

[16] M. B. Prime and A. T. DeWald, “The Contour Method,” in Practical Residual Stress Measurement Methods, G. S. Schajer, Ed. West Sussex, UK: John Wiley & Sons, Ltd, 2013, pp. 109–138.

[17] M. B. Prime and M. R. Hill, “Uncertainty, Model Error, and Order Selection for Series-Expanded, Residual-Stress Inverse Solutions,” *J. Eng. Mater. Technol.*, vol. 128, no. 2, pp. 175–185, Apr. 2006.

## TABLES

| Sample | Elastic Modulus (GPa) | Poisson's Ratio | Yield Strength (MPa) |
|---|---|---|---|
| Aluminum T-section (7085-T74) | 71 | 0.33 | 460 |
| Stainless steel DM welded plate (316L plate) | 203 | 0.3 | 440 |
| Stainless steel DM welded plate (A52 weld) | 211 | 0.289 | 345-482 |
| Titanium EB welded plate (Ti-6Al-4V) | 110 | 0.31 | 960 |
| Stainless steel forging (304L) | 200 | 0.249 | 470 |
| Nickel disk forging (Udimet-720Li) | 200 | 0.31 | 300-500 |

**Table 1: Material properties for each sample**

| Specimen | | Median (MPa) | Mean (MPa) | 75$^{th}$ percentile (MPa) | 95$^{th}$ percentile (MPa) | Max (MPa) |
|---|---|---|---|---|---|---|
| Aluminum T-section (7085-T74) | Uncertainty | 9.9 | 12.1 | 11.9 | 22 | 87.5 |
| | Repeatability | 3.7 | 5.1 | 6.2 | 12.6 | 36.7 |
| Titanium EB welded plate (Ti-6Al-4V) | Uncertainty | 12.2 | 15.8 | 14.5 | 32.5 | 298.6 |
| | Repeatability | 5.9 | 7.7 | 8.3 | 17.3 | 130.2 |
| Nickel disk forging (Udimet-720Li) | Uncertainty | 20 | 26.2 | 21.3 | 55.5 | 511.1 |
| | Repeatability | 21.5 | 24.9 | 29.7 | 51.7 | 290.9 |
| Stainless steel forging (304L) | Uncertainty | 44.9 | 57.1 | 48.7 | 132.2 | 306.6 |
| | Repeatability | 20.3 | 23.8 | 27.6 | 52.3 | 141.3 |
| Stainless steel DM welded plate | Uncertainty | 17.5 | 21.9 | 19.5 | 45.5 | 269.3 |
| | Repeatability | 14.9 | 17.3 | 21.6 | 36.3 | 146.5 |

**Table 2: Uncertainty and repeatability standard deviation statistical values**

## FIGURES

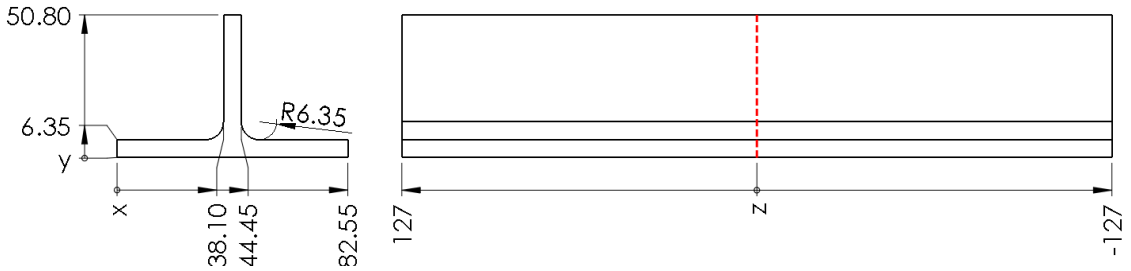


*Figure 1 – Aluminum T-section dimensions and measurement location (dimensions in mm)*

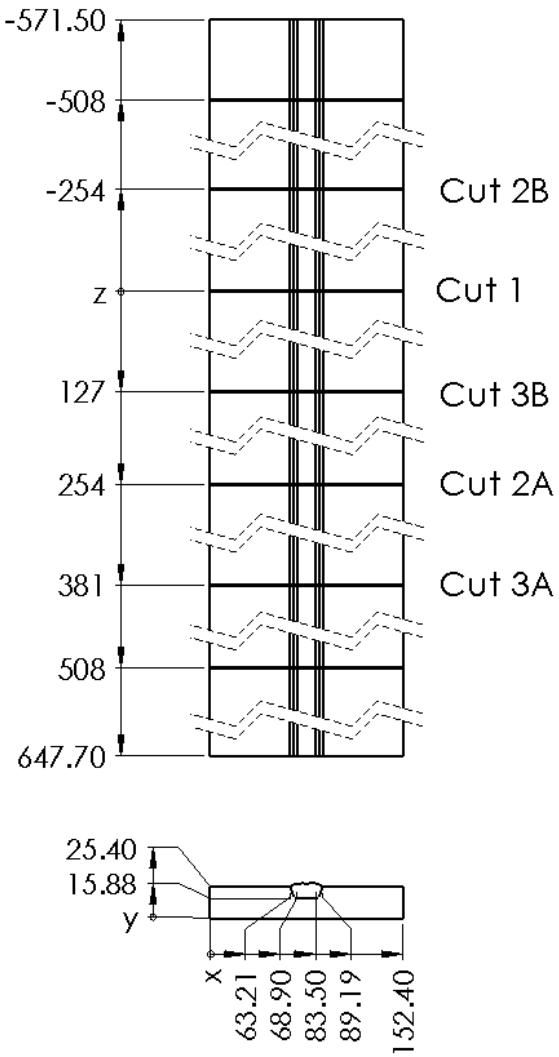


*Figure 2: Stainless steel dissimilar metal dimensions and measurement locations (dimensions in mm)*

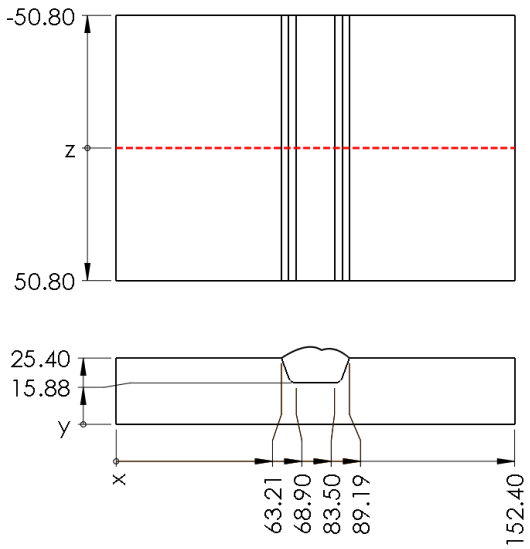


*Figure 3: Titanium electron beam welded plate dimensions and measurement location (dimensions in mm)*

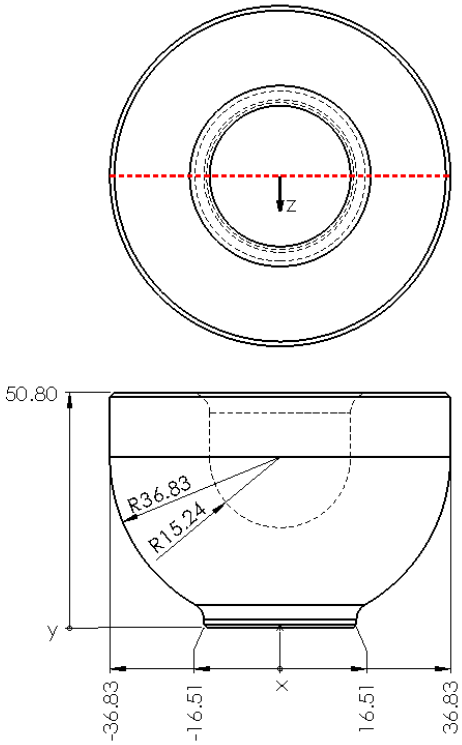


*Figure 4: Stainless steel forging dimensions and measurement location (dimensions in mm)*

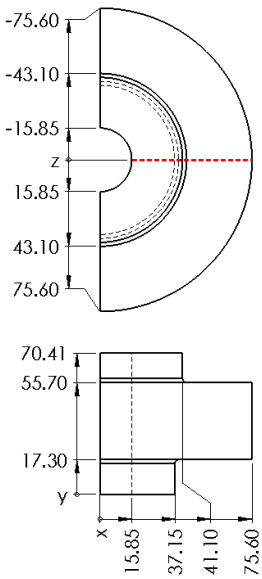


*Figure 5: Nickel disk forging dimensions and measurement location (dimensions in mm)*

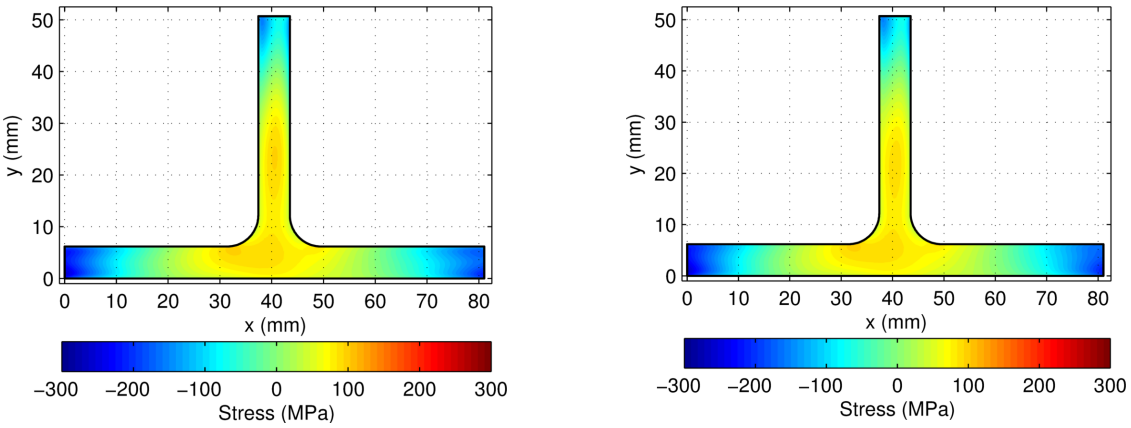


(a) (b)

*Figure 6: (a) Measured residual stress ($\sigma_{zz}$) and (b) mean of repeatability study for the aluminum T-section samples*

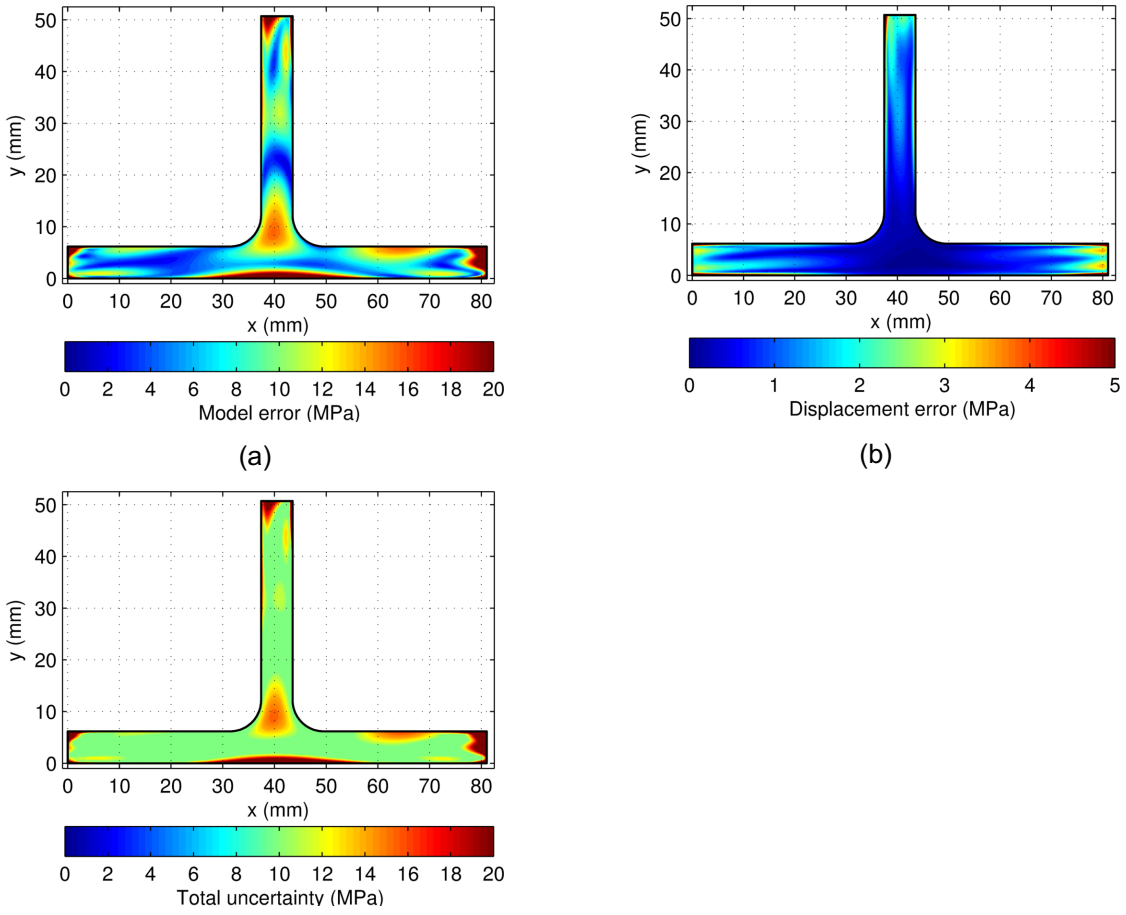


(a) (b)

(a)

*Figure 7: (a) Displacement error, (b) model error, and (c) total uncertainty for the aluminum T-section samples*

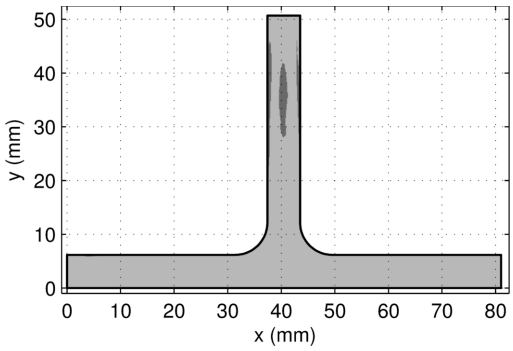


*Figure 8: Diagram of points (95.1%) where the aluminum T-section samples have a positve (light gray) and negative (dark gray) comparison between uncertainty and precision. Other measurements in the repeatability study met this criterion at 96.8%, 85.3%, 99.2%, 90.1%, 98.7%, 96.2%, 96.5%, 97.9%, and 93.0% percent of points*

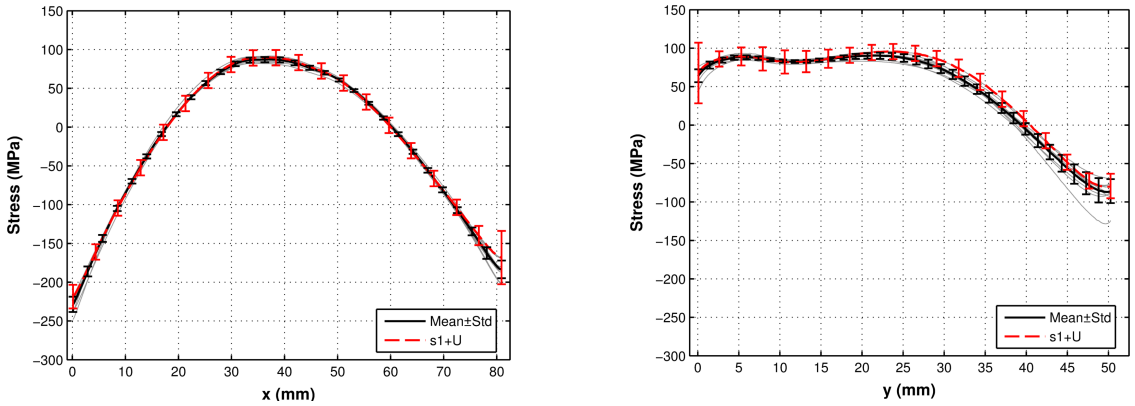


(a) (b)

*Figure 9: Line plot of the measured stress with its assocatied total uncertainty (dashed red) and the repeatability mean (solid black) for the aluminum T-section samples along the (a) x-direction at y = 3.18 mm and (b) along the y-direction at x = 40.52 mm. All other measurements are shown with thin gray lines*

(a)

(b)

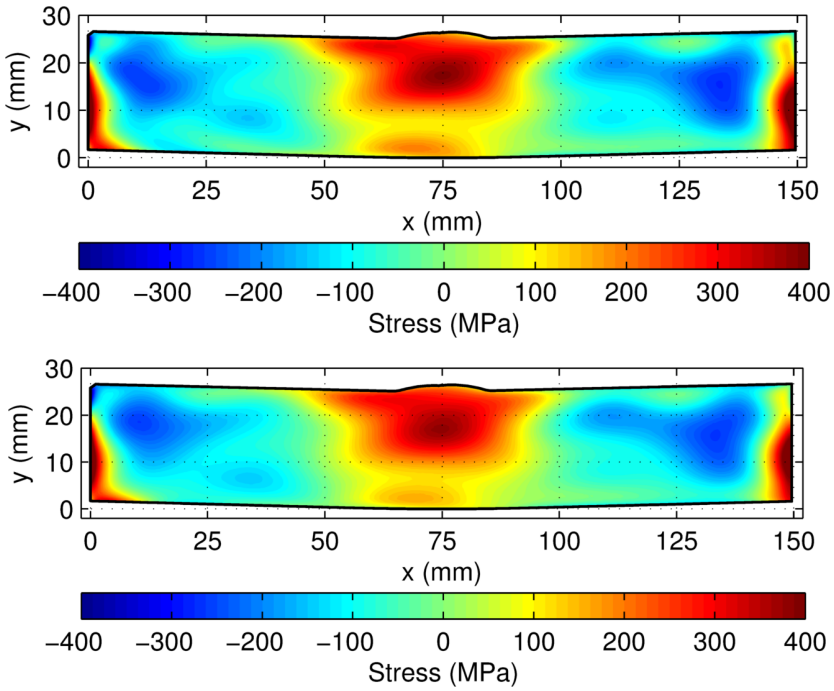


*Figure 10: (a) Measured residual stress ($\sigma_{zz}$) and (b) mean of repeatability study for the stainless steel DM welded samples*

(a)

(b)

(c)

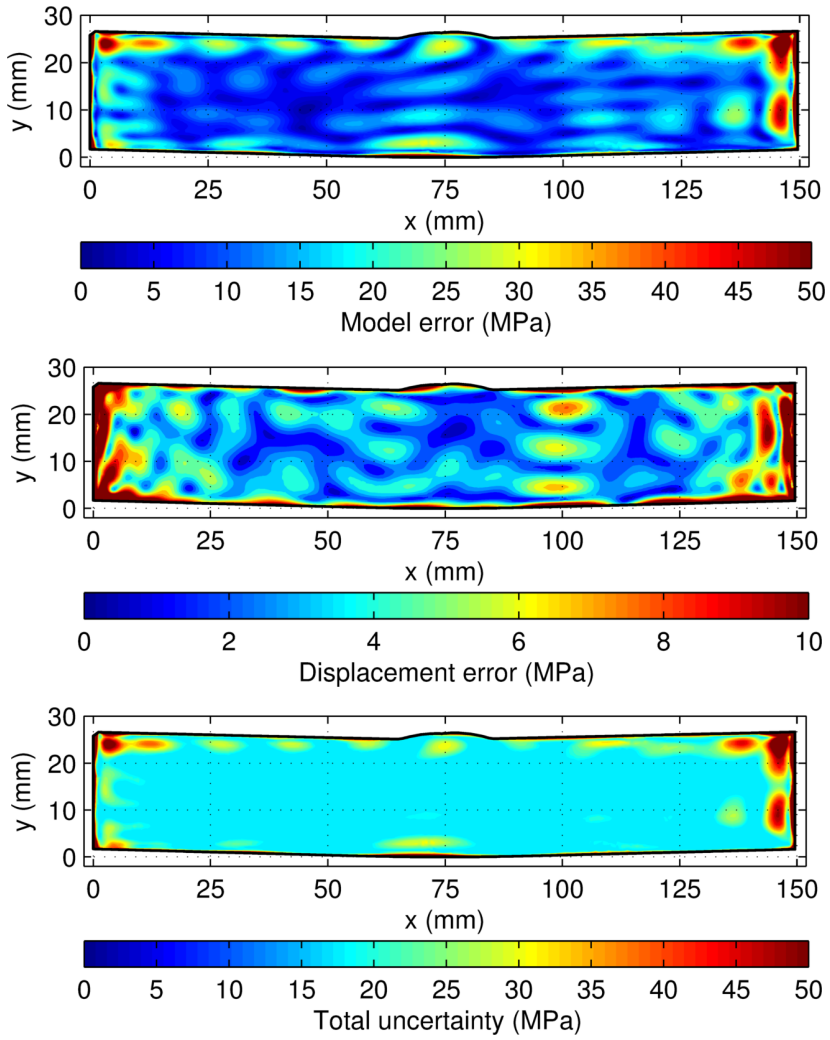


*Figure 11: (a) Displacement error, (b) model error, and (c) total uncertainty for the stainless steel DM welded samples*

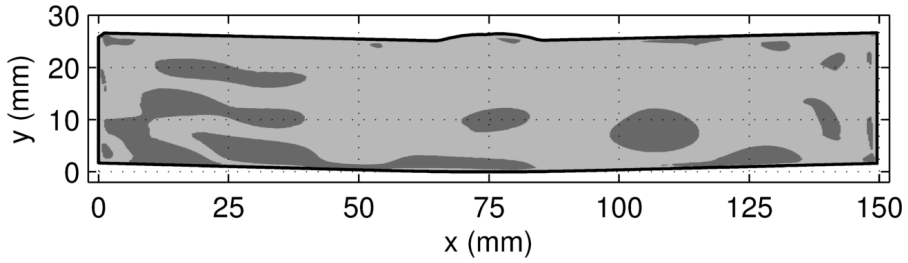


*Figure 12: Diagram of points (80.3%) where the stainless steel DM welded samples have a positve (light gray) and negative (dark gray) comparison between uncertainty and precision.*

*Other measurements in the repeatability study met this criterion at 72.8%, 73.4%, 67.4%, and 72.4% percent of points*

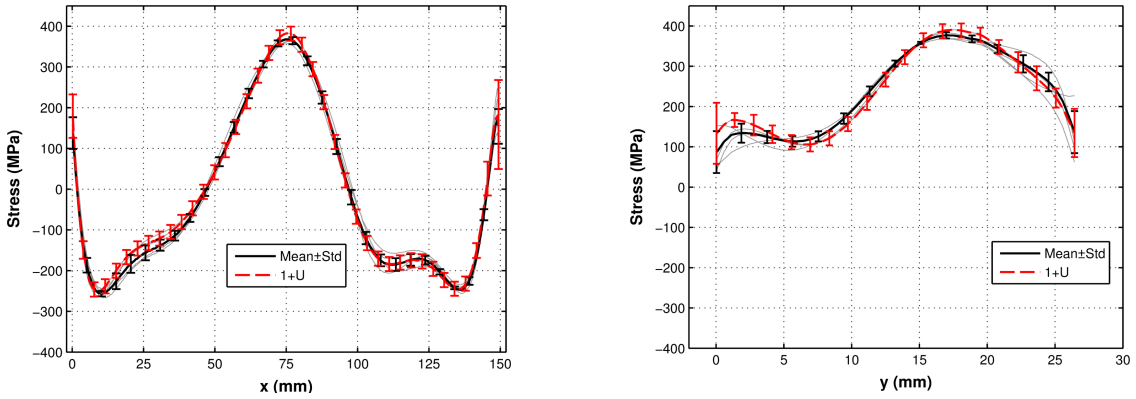


(a) (b)

*Figure 13: Line plot of the measured stress with its assocatied total uncertainty (dashed red) and the repeatability mean (solid black) for the stainless steel DM welded samples along the (a) x-direction at y = 19.05 mm and (b) along the y-direction at x = 76.2 mm. All other measurements are shown with thin gray lines*

(a)

(b)

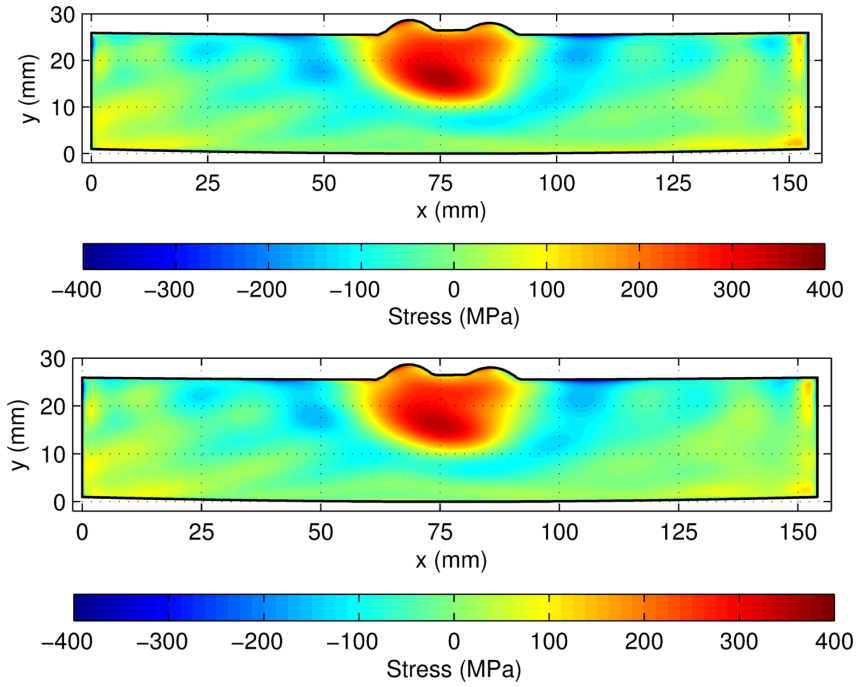


*Figure 14: (a) Measured residual stress ($\sigma_{zz}$) and (b) mean of repeatability study for the titanium EB welded plate samples*

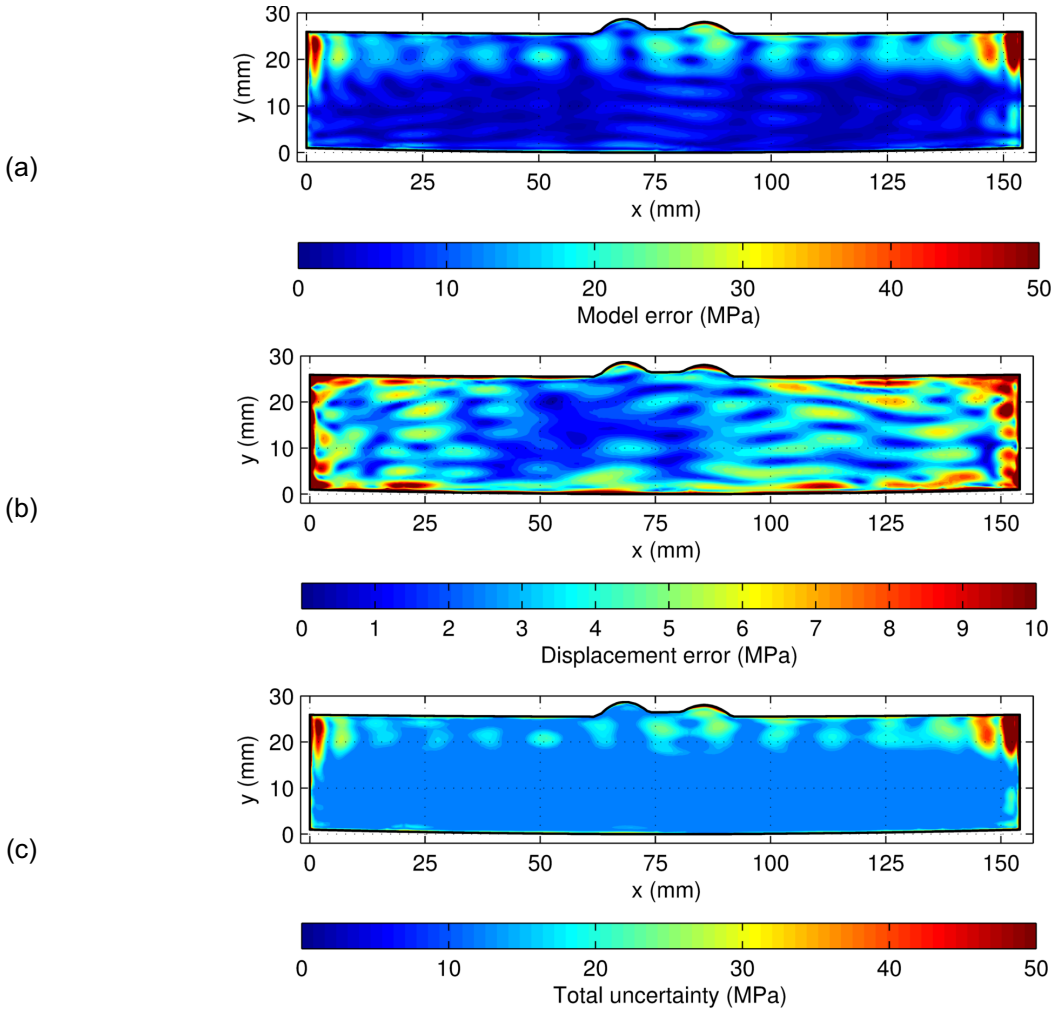


*Figure 15: (a) Displacement error, (b) model error, and (c) total uncertainty for the titanium EB welded plate samples*

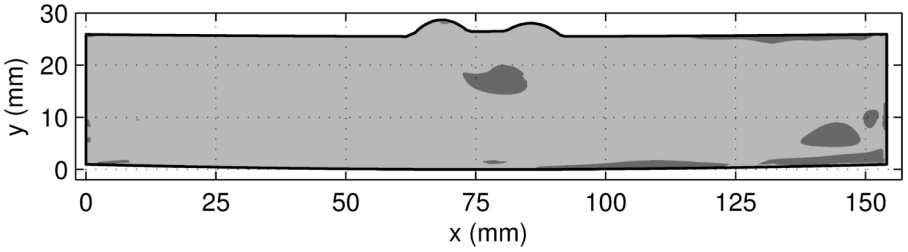


*Figure 16: Diagram of points (94.5%) where the titanium EB welded plate samples have a positve (light gray) and negative (dark gray) comparison between uncertainty and precision.*

*Other measurements in the repeatability study met this criterion at 97.0%, 92.1%, 98.0%, 98.0%, and 95.7% percent of points*

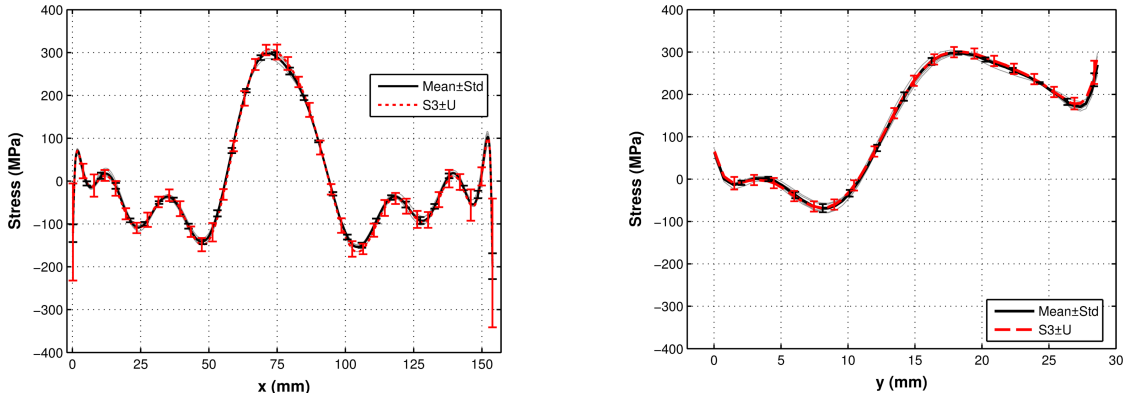


(a) (b)

*Figure 17: Line plot of the measured stress with its assocatied total uncertainty (dashed red) and the repeatability mean (solid black) for the titanium EB welded plate samples along the (a)*

*x-direction at y = 20.32 mm and (b) along the y-direction at x = 68.15 mm. All other measurements are shown with thin gray lines*

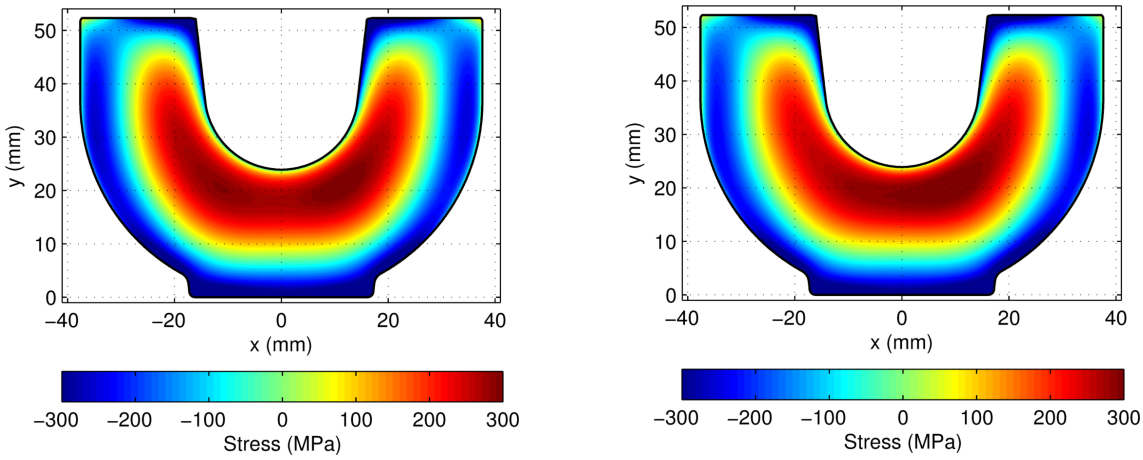


*Figure 18: (a) Measured residual stress ($\sigma_{zz}$) and (b) mean of repeatability study for the stainless steel forging samples*

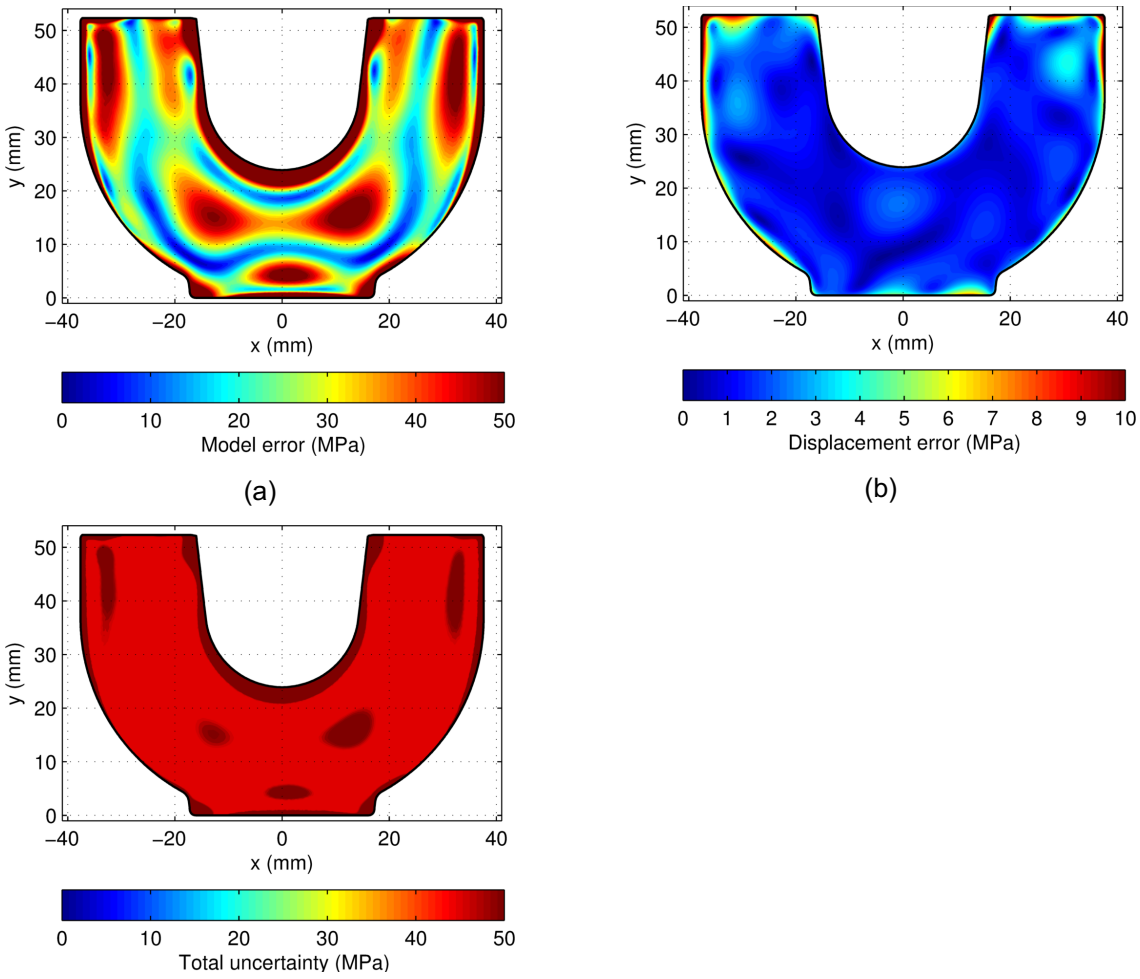


*Figure 19: (a) Displacement error, (b) model error, and (c) total uncertainty for the stainless steel forging samples*

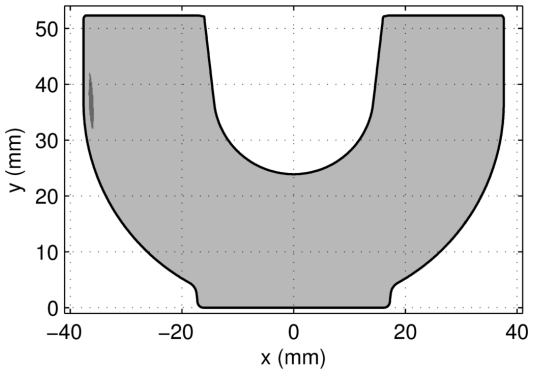


*Figure 20: Diagram of points (99.8%) where the stainless steel forging samples have a positve (light gray) and negative (dark gray) comparison between uncertainty and precision. Other*

*measurements in the repeatability study met this criterion at 98.8%, 96.6%, 91.4%, and 97.9% percent of points*

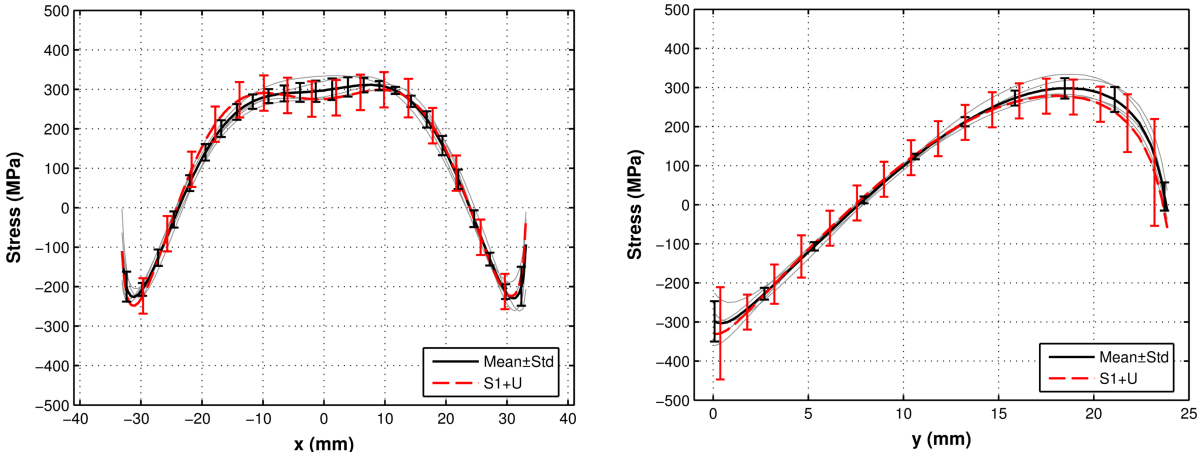


(a) (b)

*Figure 21: Line plot of the measured stress with its assocatied total uncertainty (dashed red) and the repeatability mean (solid black) for the stainless steel forging samples along the (a) x-direction at y = 19.05 mm and (b) along the y-direction at x = 0. All other measurements are shown with thin gray lines*

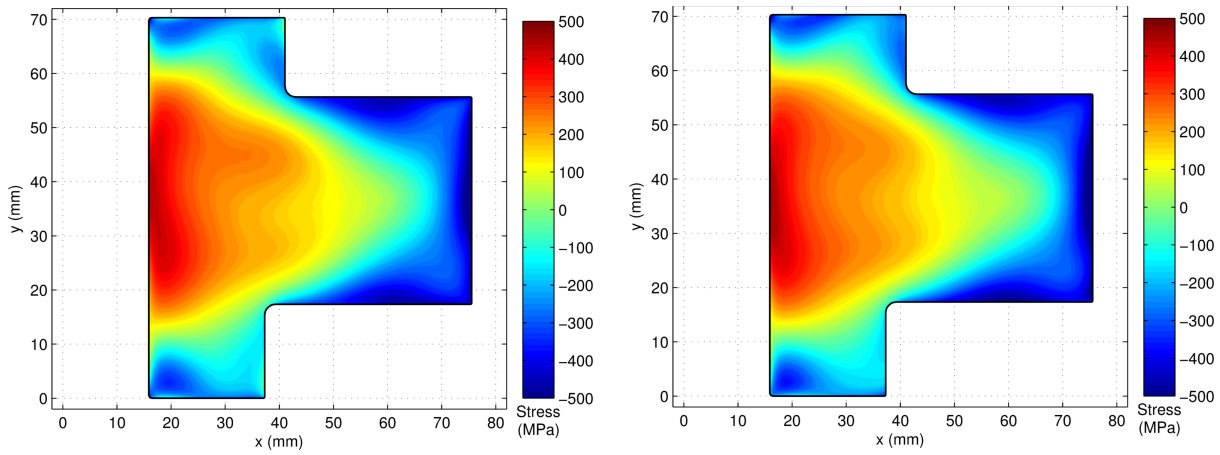


*Figure 22: (a) Measured residual stress ($\sigma_{zz}$) and (b) mean of repeatability study for the nickel disk forging samples*

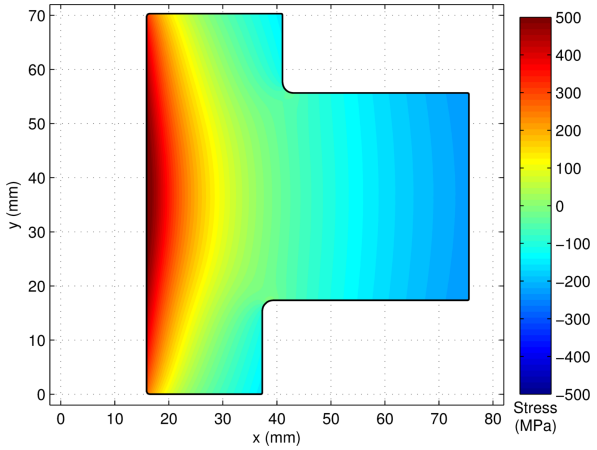


*Figure 23: Stress release when sectioning the nickel disk forging samples in half*

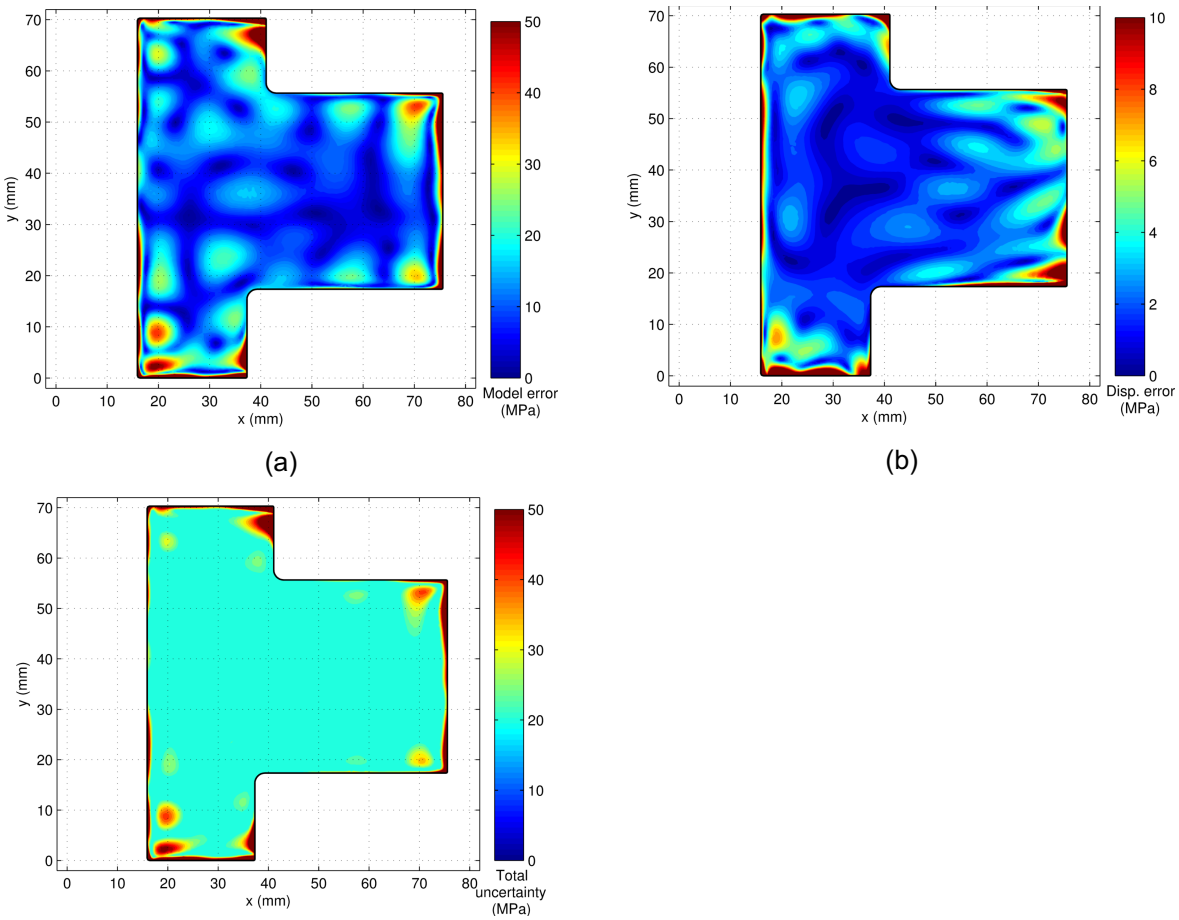


*Figure 24: (a) Displacement error, (b) model error, and (c) total uncertainty for the nickel disk forging samples*

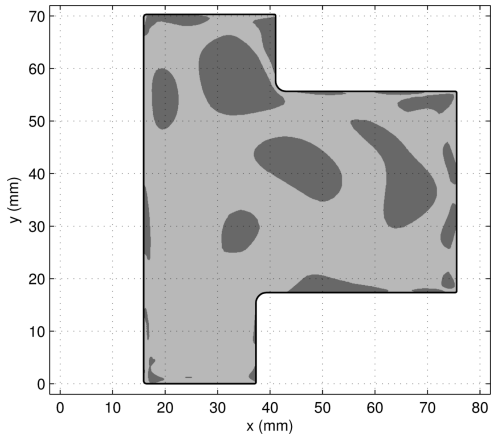


*Figure 25: Diagram of points (76.2%) where the nickel disk forging samples have a positve (light gray) and negative (dark gray) comparison between uncertainty and precision. Other*

*measurements in the repeatability study met this criterion at 53.0%, 50.0%, 64.8%, 73.1%, and 76.6% percent of points*

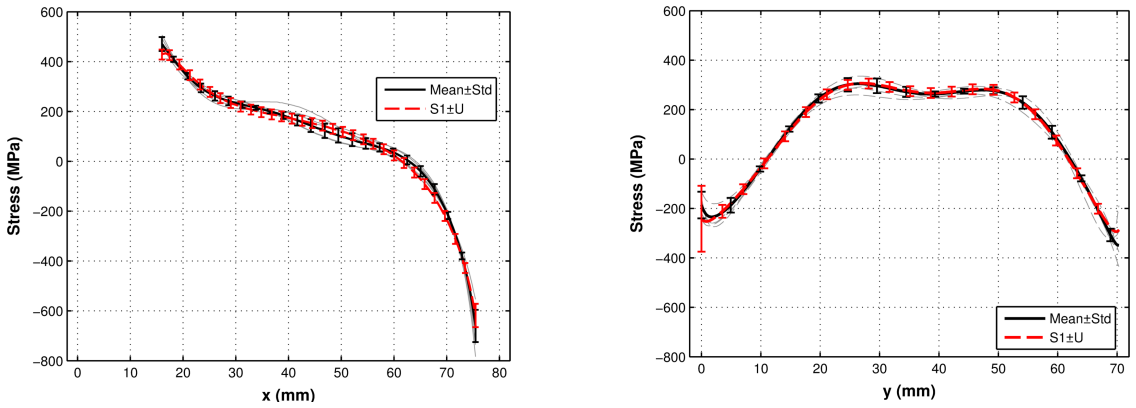


(a) (b)

*Figure 26: Line plot of the measured stress with its assocatied total uncertainty (dashed red) and the repeatability mean (solid black) for the nickel disk forging samples along the (a) x-direction at y = 35.15 mm and (b) along the y-direction at x = 25.4 mm. All other measurements are shown with thin gray lines*

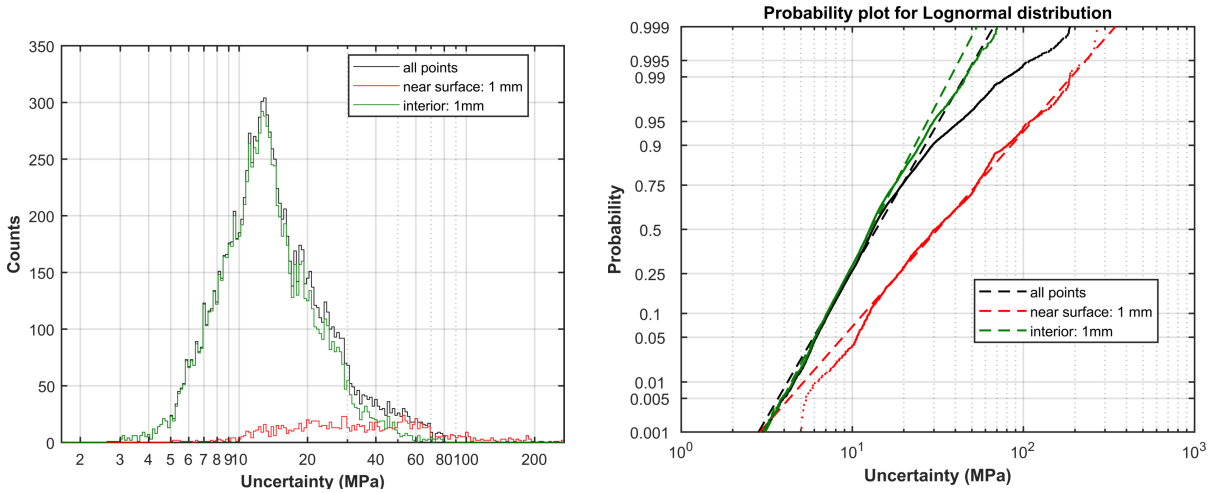


(a) (b)

*Figure 27: Uncertainty estimate prior to adding the uncertainty floor for the for the stainless steel DM welded samples (a) histogram and (b) probability plot (the dashed lines show a lognormal distribution and the points show the distribution of the data)*

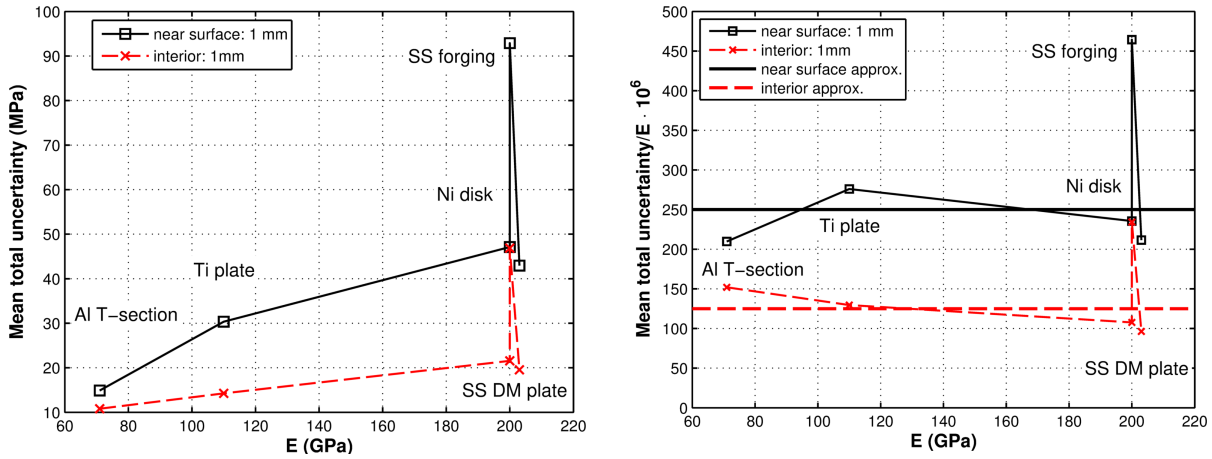


*Figure 28: (a) Line plot of the near surface points (within 1 mm of the part boundary, solid black line) and the interior points (futher than 1 mm from the part boundary, dashed red line) of the uncertainty estimate as a function of elatic modulus and (b) normalized by elastic modulus*